Dynamical screening at simple-metal surfaces

A. Liebsch

Institut für Festkörperforschung der Kernforschungsanlage Jülich, D-5170 Jülich, Federal Republic of Germany

The dynamic image plane in the long-wavelength limit has been calculated within the time-dependent density-functional approach for several simple-metal surfaces. Using the dynamical force sum rule it is proven that the image plane is given by the first moment of the induced density in the region outside the positive background. The imaginary part of the centroid $d(\omega)$ of the screening charge, which determines the probability for electron-hole pair excitations at the surface, is linear in ω up to about one-half of the work function and then rises steeply near the vacuum threshold. Close to 0.8 of the bulk plasma frequency $\mathrm{Im}d(\omega)$ shows a peak which becomes very sharp for low bulk densities. If the response to the applied field is treated within the random-phase approximation, the spectral weight of $\mathrm{Im}d(\omega)$ is shifted almost uniformly to higher frequencies. It is also found that the linear coefficient of $\mathrm{Im}d(\omega)$ at low frequencies is in excellent agreement with the quasistatic predictions based on the golden-rule formula.

I. INTRODUCTION

The dynamic screening properties of metal surfaces have in recent years received considerable attention because of their importance for many surface spectroscopies.[1] In the long-wavelength limit, the key quantity that characterizes the electronic response to the applied electromagnetic fields is the centroid $d(\omega)$ of the screening density induced by a uniform electric field oriented perpendicular to the surface. Among the quantities that are directly determined by $d(\omega)$ are the surface photoelectric yield, the linear coefficient of the surface plasma dispersion relation, the electronic lifetime of adsorbate vibrations, nonlocal corrections to the Fresnel equations, and the van der Waals reference plane.[2]

Despite this wide-ranging significance of the function $d(\omega)$, only limited information on it is available today, even for simple metals. So far, the most realistic calculations for semi-infinite jelliumlike metals were carried out by Feibelman[1,3] for frequencies ranging from $0.6\omega_p$ to about $1.3\omega_p$, where ω_p is the bulk plasma frequency ($\omega_p^2 = 4\pi\bar{n}$, $\bar{n}$ is the bulk density). The ground-state electronic properties were determined with use of density-functional theory while the response to the external fields was treated within the random-phase approximation (RPA). The validity of this approach was convincingly demonstrated by the excellent agreement that was achieved with measured photoyield spectra for Al by the data were taken by Levinson and Plummer.[4] Aside from the unknown behavior of $d(\omega)$ at lower frequencies (apparently, the solution of the response equations in this range failed because of numerical difficulties), there remained the question as to what extent exchange-correlation contributions to the local field might influence the frequency dependence of $d(\omega)$. It was recently shown that a consistent treatment of electron-electron interactions in the ground state and in the presence of the external perturbation is required in order to satisfy various exact sum rules.[5]

The purpose of this work is to present results for $d(\omega)$ for several simple metals ($r_s = 2$, 3, 4, and 5 where $r_s^{-3} = 4\pi\bar{n}/3$) over the entire frequency range below ω_p. The formalism is based on the time-dependent density-functional approach[6,7] and amounts to a direct solution of the linear-response equations. The smoothness of the electron profile at the surface and the nonlocal nature of the response to the applied field are fully included. Since electron interactions in the presence and in the absence of the perturbing field are treated on the same footing [the local-density approximation (LDA) is used], the static force sum rule and the so-called surface f-sum rule are satisfied automatically and, at low frequencies, $d(\omega)$ smoothly approaches its known value in the static limit. Our solution of the response equations is complementary to that of Kempa and Schaich,[8] who solve them in Fourier space. The formal procedure is analogous to that employed previously[9] to determine the induced density at imaginary frequencies which is relevant for the evaluation of the van der Waals reference plane.[10] The response at purely imaginary frequencies is, however, much simpler in the sense that the induced density $\delta n(z,iu)$ remains real and exhibits in the interior of the metal only one Friedel oscillation which is independent of frequency u. Thus a direct determination of the centroid of $\delta n(z,iu)$ is feasible. At real frequencies, on the other hand, $\delta n(z,\omega)$ is complex and consists in the interior of a complicated superposition of several Friedel oscillations.[3]

In order to be able to determine the centroid of $\delta n(z,\omega)$ we use the dynamic force sum rule which was recently derived by Sorbello[11] for atoms and small metal particles. We first apply this rule to thin metal slabs and then generalize it to the case of a semi-infinite system. We show that, as a result of this sum rule, a condition can be found which relates the first moment of the induced density in the interior of the metal to the first moment outside the edge of the positive background. Thus the centroid $d(\omega)$ is in fact completely determined by

the spatial distribution of $\delta n(z,\omega)$ outside the metal. In the static limit, such a condition is known to hold as a result of the static force sum rule.[12] At finite real frequencies, this relationship is very useful indeed, since it circumvents the evaluation of the first moment of the oscillatory interior part of the induced density. As a consequence of the dynamic force sum rule, the frequency-dependent image plane can be identified with the first moment of the induced density in the exterior of the metal.

Qualitatively, the response function $d(\omega)$ below the bulk plasma frequency shows the following behavior. At low frequencies up to about one-half of the work function, $\mathrm{Im}d(\omega)$ is approximately linear in ω. The slope decreases by about 1 order of magnitude as r_s increases from 2 to 5. In the vicinity of the threshold for emission, $\mathrm{Im}d(\omega)$ rises steeply, indicating a large increase in the number of channels for electron-hole pair excitations in the region of the surface barrier. Above threshold, $\mathrm{Im}d(\omega)$ shows a maximum close to $0.8\omega_p$ for all bulk densities that we have considered. This feature is less pronounced in the case of high-density metals $(r_s=2)$ but becomes extremely sharp for lower bulk densities $(r_s \geq 4)$. The induced density at this resonance has monopole character and is spatially not more localized in the surface region than at other frequencies.

We have checked our earlier calculations[9,10,13] at imaginary frequencies by making use of the dynamical force sum rule. Although the new absolute values of $d(iu)$ agree with the old results to within about one percent, the linear coefficient ξ at low frequencies is now smaller. As expected, this coefficient is the same as that of $\mathrm{Im}d(\omega)$ in the limit of small frequencies. In fact, we now find that ξ agrees well with the quasistatic prediction[14] based on the golden rule if the full self-consistent surface potential (i.e., including exchange-correlation terms) together with the bulk potential is used.[9]

In order to investigate the importance of exchange and correlation for the frequency dependence of $d(\omega)$ we have carried out RPA-type response calculations, retaining, however, the LDA for the ground state. At those frequencies and bulk densities where a comparison is possible our results agree very well with those of Feibelman.[1,4] In general, we find $\mathrm{Im}d(\omega)$ to be somewhat smaller than in the consistent LDA response treatment. Also, the peak near $0.8\omega_p$ is less pronounced in the RPA and tends to lie at slightly higher frequencies. A shift of spectral weight to higher frequencies as a result of the neglect of exchange-correlation contributions to the effective potential is to be expected because of the less attractive potential in the region of the induced density.[5]

The structure of this paper is as follows. In Sec. II we introduce the key quantities characterizing the response at a metal surface and review the finite-frequency extension of the density-functional approach. The dynamical force sum rule for semi-infinite systems will be derived in Sec. III and details of the computational procedure are given in Sec. IV. Section V contains the discussion of our results and the conclusions are presented in Sec. VI. Atomic units are used throughout this paper unless noted otherwise.

II. DENSITY-FUNCTIONAL RESPONSE

Let us consider the interaction of the metal electrons (the positive background occupies the half-space $z \leq 0$) with the external electric potential

$$\phi_{\mathrm{ext}}(\mathbf{r},\omega) = -\frac{2\pi}{q}\exp(i\mathbf{q}_\parallel\cdot\mathbf{r}_\parallel + qz + i\omega t) , \tag{1}$$

with $q = |\mathbf{q}_\parallel|$. For sufficiently weak external perturbations the Fourier components of the induced density are given by

$$\delta n(z,q,\omega) = \int dz' \, \mathcal{X}(z,z',q,\omega)\phi_{\mathrm{ext}}(z',q,\omega) , \tag{2}$$

where $\mathcal{X}$ is the density repsonse function of the semi-infinite metal. Far from the surface the induced Coulomb potential has the form

$$\delta\phi(z,q,\omega) = \frac{2\pi}{q} \int dz' \, e^{-q|z-z'|} \, \delta n(z',q,\omega)$$

$$\rightarrow \frac{2\pi}{q}e^{-qz}g(q,\omega), \quad z \gg 0 , \tag{3}$$

where the response function $g(q,\omega)$ is defined as

$$g(q,\omega) = \int dz \, e^{qz}\delta n(z,q,\omega)$$

$$= -\frac{2\pi}{q} \int dz \int dz' e^{qz}e^{qz'}\mathcal{X}(z,z',q,\omega) . \tag{4}$$

In the long-wavelength limit, g has the expansion[1,3,15]

$$g(q,\omega) = \sigma(\omega)\left[1 + 2q\frac{\epsilon(\omega)}{\epsilon(\omega)+1}d(\omega) + O(q^2)\right] , \tag{5}$$

where

$$\sigma(\omega) = \int dz \, \delta n(z,0,\omega) = \frac{\epsilon(\omega)-1}{\epsilon(\omega)+1} \tag{6}$$

is the total surface charge induced by a uniform, frequency-dependent electric field oriented perpendicular to the surface and $d(\omega)$ is the centroid of this density

$$d(\omega) = \int dz \, z \, \delta n(z,0,\omega)/\sigma(\omega) . \tag{7}$$

Equation (6) follows from the standard textbook treatment of the dielectric response at a metal surface where the bulk is characterized by a local dielectric function $\epsilon(\omega)$.

As shown by Persson and Zaremba,[14] the imaginary part of the response function $g(q,\omega)$ is proportional to the rate of exciting electron-hole pairs at the surface (A is the surface area):

$$w = \frac{Aq}{\pi\hbar}\left[\frac{2\pi}{q}\right]^2 \mathrm{Im}g(q,\omega) . \tag{8}$$

Thus in the long-wavelength limit, w is determined by the imaginary part of the induced charge centroid:

$$w = \frac{4\pi A}{\hbar}\sigma(\omega)\frac{2\epsilon(\omega)}{\epsilon(\omega)+1}\mathrm{Im}d(\omega) + \cdots . \tag{9}$$

On the other hand, the transition rate w may be calculated with use of the golden-rule formula[14]

$$w = 2\frac{2\pi}{\hbar} \int d^3k \int d^3k' f_k(1-f_{k'}) |\langle k' | \phi_{\text{SCF}} | k \rangle|^2$$

$$\times \delta(\epsilon_{k'} - \epsilon_k - \hbar\omega) , \tag{10}$$

where the initial factor 2 accounts for the electron spin and ϕ_{SCF} is the total complex potential. f_k are Fermi-Dirac occupation factors.

Within the time-dependent extension of the density-functional approach,[6,7] the induced potential consists of Coulomb as well as exchange-correlation contributions. Thus in the limit $q \rightarrow 0$ one has

$$\phi_{\text{SCF}}(z,\omega) = \phi_{\text{ext}}(z,\omega) + \delta\phi(z,\omega) + \delta V_{\text{xc}}(z,\omega) , \tag{11}$$

where $\phi_{\text{ext}}(z,\omega) = -2\pi z$ and

$$\delta\phi(z,\omega) = \int dz' e^{-\kappa|z-z'|} \left[\frac{2\pi}{\kappa} \delta n(z',\omega) + \frac{\kappa}{2} \delta\phi(z',\omega) \right] , \tag{12}$$

$$\delta V_{\text{xc}}(z,\omega) = \frac{\partial V_{\text{xc}}}{\partial n} \bigg|_{n=n_0(z)} \delta n(z,\omega) . \tag{13}$$

Equation (12) implies $\delta\phi''(z,\omega) = -4\pi\delta n(z,\omega)$ regardless of the value of κ.[16] This expression of the Coulomb potential is useful, since it allows explicit handling of the asymptotic form of $\delta\phi(z,\omega)$ and since the short-range kernel in (12) suppresses all long-range potentials due to finite surface charges.

The induced density is related to the self-consistent potential via the independent-particle susceptibility χ_0:

$$\delta n(z,\omega) = \int dz' \chi_0(z,z',\omega) \phi_{\text{SCF}}(z',\omega) . \tag{14}$$

The single-particle energies and wave functions that are used to construct χ_0 should be derived from the same exchange-correlation functional as that used in Eq. (13). Of course, this response approach is approximate, since only the static (local) functional is used, whereas, in principle, the response kernel should also be frequency dependent. Nevertheless, as long as the same functional is employed to determine both the ground-state electronic properties of the metal and its response to the external field, two exact sum rules are satisfied that relate the first and first inverse frequency moment of $d(\omega)$ to ground-state quantities. Thus the accuracy of these moments depends only on the quality of the static exchange-correlation potential.[5]

Once the induced density $\delta n(z,\omega)$ is obtained from the closed set of response equations (11)–(14), the centroid $d(\omega)$ can, in principle, be calculated directly using the definition (7). A more elegant, and for practical purposes considerably more useful, equivalent expression can be derived from the dynamical force sum rule. This is the topic of the following section.

III. DYNAMICAL FORCE SUM RULE

It has recently been shown by Sorbello[11] that the well-known static force sum rule which follows from the Hellman-Feynman theorem can be generalized to the dynamical case. Let us consider a finite electronic sys-

tem subject to a uniform electric field that oscillates in time at a frequency ω. As a result of the sum rule, the instantaneous force acting on the ionic charges is directly proportional to the frequency-dependent electronic polarizability of the system. Expressing the latter quantity in terms of the induced density $\delta n(\mathbf{r},\omega)$, one obtains the relationship[11]

$$\int d^3r\, n_+(\mathbf{r})\nabla\phi(\mathbf{r},\omega) = \omega^2 \int d^3r\, \mathbf{r}\, \delta n(\mathbf{r},\omega) , \tag{15}$$

where $n_+(\mathbf{r})$ is the number density of the positive ions and $\phi(\mathbf{r},\omega)$ is the total Coulomb potential acting on the electrons, i.e., ϕ consists of the external potential plus the Hartree term $\delta\phi(\mathbf{r},\omega)$ induced by $\delta n(\mathbf{r},\omega)$.

Let us now consider a slab of thickness L whose uniform positive background of density $\bar{n}$ extends from $z = -L/2$ to $z = +L/2$, and which is placed symmetrically between two oppositely charged capacitor plates. Because of the translational symmetry parallel to the surface, we obtain from Eq. (15) the condition

$$\phi(z=L/2, \omega) = 4\pi\bar{\omega}^2 \int_0^\infty dz\, z\, \delta n(z,\omega) , \tag{16}$$

where we have used the fact that both $\phi(z,\omega)$ and $\delta n(z,\omega)$ are odd functions of z and $\bar{\omega} \equiv \omega/\omega_p$. This relationship may be conveniently rewritten as

$$\phi(L/2,\omega) = 4\pi\bar{\omega}^2 \sigma_L(\omega)[L/2 + d_L(\omega)] , \tag{17}$$

where $\sigma_L(\omega)$ is the integrated weight of the charge induced in the right half of the slab and $d_L(\omega)$ is the centroid measured from the right-hand jellium edge:

$$\sigma_L(\omega) = \int_0^\infty dz\, \delta n(z,\omega) , \tag{18}$$

$$d_L(\omega) = \int_0^\infty dz(z - L/2)\delta n(z,\omega)/\sigma_L(\omega) . \tag{19}$$

On the other hand, if we express $\phi(z,\omega)$ as a superposition of applied and induced potential, the left-hand side of Eq. (16) can be written as

$$\phi(L/2,\omega) = \phi_{\text{ext}}(L/2,\omega) + \delta\phi(L/2,\omega)$$
$$= -4\pi\sigma_0 L/2$$
$$\quad -2\pi \int_{-\infty}^\infty dz' |L/2 - z'| \delta n(z',\omega) , \tag{20}$$

where σ_0 is the positive charge per unit area on the right-hand capacitor plate. After some algebraic manipulation, this leads to

$$\phi(L/2,\omega) = -2\pi L[\sigma_0 - \sigma_L(\omega)]$$
$$\quad + 4\pi\sigma_L(\omega)[d_L(\omega) - a_L(\omega)] , \tag{21}$$

where

$$a_L(\omega) = \int_{L/2}^\infty dz(z - L/2)\delta n(z,\omega)/\sigma_L(\omega) . \tag{22}$$

From Eqs. (17) and (21) we obtain the condition

$$(1 - \bar{\omega}^2)d_L(\omega) - a_L(\omega) = (L/2)[\sigma_0/\sigma_L(\omega) - 1 + \bar{\omega}^2] . \tag{23}$$

Thus, as a result of the dynamical force sum rule, the centroid $d_L(\omega)$ of the induced density is actually determined by the quantity $a_L(\omega)$, i.e., by the moment of

$\delta n(z,\omega)$ outside the edge of the positive background.

Now let us assume that L becomes very large. Since the induced density (below ω_p) remains localized on the two sides of the slab, the potential in the interior approaches

$$\phi(z,\omega) = -4\pi[\sigma_0 - \sigma_L(\omega)]z \; , \tag{24}$$

while far in the vacuum on the right it takes the form

$$\phi(z,\omega) = -4\pi\{\sigma_0 z - \sigma_L(\omega)[L/2 + d_L(\omega)]\} \; . \tag{25}$$

Thus the ratio of internal to external electric field becomes

$$E(\text{in})/E(\text{out}) = 1 - \sigma_L(\omega)/\sigma_0 = [\epsilon(\omega)]^{-1} \; . \tag{26}$$

If we represent $\epsilon(\omega)$ by the Drude dielectric function, we find

$$\sigma_L(\omega)/\sigma_0 = 1/(1 - \bar{\omega}^2) \tag{27}$$

for large L. In this limit we therefore obtain from Eq. (23)

$$d_L(\omega) = a_L(\omega)/(1 - \bar{\omega}^2)$$

$$= a_L(\omega)\sigma_L(\omega)/\sigma_0 \; . \tag{28}$$

Let us now choose

$$\sigma_0 = \epsilon(\omega)/[\epsilon(\omega) + 1] \tag{29}$$

so that

$$\sigma_L(\omega) = \sigma(\omega) = \frac{\epsilon(\omega) - 1}{\epsilon(\omega) + 1} \tag{30}$$

for L large. Thus the total weight of the charge induced at the surface of the slab equals that induced at the surface of a semi-infinite metal by an external capacitor plate of unit positive charges. From (19), (22), and (28) we then have

$$d_L(\omega) = \frac{\epsilon(\omega) + 1}{\epsilon(\omega)} \int_0^\infty dz\, z\, \delta n(z,\omega) \; , \tag{31}$$

where we now have placed the origin of the z axis at the right-hand jellium edge. If we assume that, below ω_p, the profile of the induced density at the slab surface approaches for large L that at the semi-infinite metal surface, Eq. (31) also holds in the latter case, i.e.,

$$d(\omega) = \int_{-\infty}^{\infty} dz\, z\, \delta n(z,\omega)/\sigma(\omega)$$

$$= \frac{\epsilon(\omega) + 1}{\epsilon(\omega)} \int_0^\infty dz\, z\, \delta n(z,\omega) \; . \tag{32}$$

The dynamical image plane[1] is then simply given by the first moment of the induced density outside the jellium edge:

$$d_{\text{IP}}(\omega) = \frac{\epsilon(\omega)}{\epsilon(\omega) + 1} d(\omega)$$

$$= \int_0^\infty dz\, z\, \delta n(z,\omega) \; . \tag{33}$$

Equation (32) is the main result of this section. It shows that, in order to evaluate the centroid of the

dynamically induced density, it actually suffices to know the density in the exterior. Equivalently, the first moment of $\delta n(z,\omega)$ in the interior is simply related to its first moment outside the jellium edge:

$$\int_{-\infty}^0 dz\, z\, \delta n(z,\omega) = \frac{-1}{\epsilon(\omega)} \int_0^\infty dz\, z\, \delta n(z,\omega) \; . \tag{34}$$

In the static limit, this gives the well-known result[12]

$$\int_{-\infty}^0 dz\, z\, \delta n(z,0) = 0 \; , \tag{35}$$

i.e., since $\sigma(\omega = 0) = 1$,

$$d(0) = \int_0^\infty dz\, z\, \delta n(z,0) \; . \tag{36}$$

It is convenient to introduce the normalized induced density

$$f(z,\omega) = \delta n(z,\omega)/\sigma(\omega) \; , \tag{37}$$

i.e., its integrated weight is unity independently of ω. If we define its external moment as

$$f(\omega) = \int_0^\infty dz\, zf(z,\omega) \; , \tag{38}$$

we have from (32) the relation

$$d(\omega) = \frac{\epsilon(\omega) - 1}{\epsilon(\omega)} f(\omega)$$

$$= \frac{1}{1 - \bar{\omega}^2} f(\omega) \; . \tag{39}$$

Thus, according to Feibelman,[1] the photoyield at a metal surface for p-polarized light incident at 45° is given by (a.u.)

$$Y(\omega) = \sqrt{8}\alpha\omega \, \text{Im} f(\omega) \; , \tag{40}$$

where α is the fine-structure constant.

Let us return for a moment to the case of a slab of large but finite thickness, and let us define bulk and surface contributions to the total Coulomb potential according to

$$\phi(z,\omega) = \phi_b(z,\omega) + \phi_s(z,\omega) \; , \tag{41}$$

where ϕ_b is given by (24) and σ_0 and $\sigma_L(\omega)$ are specified in Eqs. (29) and (30):

$$\phi_b(z,\omega) = -4\pi z/[\epsilon(\omega) + 1] \; . \tag{42}$$

Since, for large L,

$$\bar{\omega}^2 \sigma_L(\omega) = -1/[\epsilon(\omega) + 1] \; , \tag{43}$$

we obtain from Eq. (17) the following condition for the surface potential ϕ_s at the jellium edge:

$$\phi_s(L/2,\omega) = 4\pi\bar{\omega}^2\sigma(\omega)d(\omega) \; . \tag{44}$$

In the case of the semi-infinite metal, it is convenient to define

$$\phi_{\text{ext}}(z,\omega) = -2\pi[z - d(\omega)] \tag{45}$$

so that

$$\phi(z,\omega) = \phi_{\text{ext}}(z,\omega) + \delta\phi(z,\omega)$$

$$\rightarrow -2\pi[1 \pm \sigma(\omega)][z - d(\omega)] \tag{46}$$

for $z \gg 0$ (upper sign) and $z \ll 0$ (lower sign). Defining again

$$\phi(z,\omega) = \phi_b(z,\omega) + \phi_s(z,\omega) , \tag{47}$$

with

$$\phi_b(z,\omega) = -2\pi[1 - \sigma(\omega)][z - d(\omega)] \tag{48}$$

for all z, we obtain

$$\phi_b(z = 0, \omega) = 2\pi[1 - \sigma(\omega)]d(\omega)$$
$$= -4\pi \bar{\omega}^2 \sigma(\omega) d(\omega) . \tag{49}$$

Thus, if we assume that the density induced at the surface of a very thick slab approaches that induced at a semi-infinite metal surface, the corresponding surface contribution to the Coulomb potential will be the same. Equation (44) then also holds for the semi-infinite case and we find

$$\phi(z = 0, \omega) = 0 . \tag{50}$$

With the definition of ϕ_{ext} given in Eq. (45), the force sum rule thus implies that the Coulomb part of the complex local potential must vanish at the jellium edge. In the static limit, this condition had been shown previously to hold for small metal spheres, jellium slabs, and semi-infinite systems.[12]

We close this section by pointing out that the force sum rule is satisfied only if electron-electron interactions in the presence of the perturbing potential are treated on the same level of approximation as in the ground state. In the time-dependent density-functional approach this is automatically the case. The LDA-based RPA response treatment, on the other hand, amounts to a time-dependent Hartree theory with the LDA ground-state local exchange-correlation potential $V_{\text{xc}}(\mathbf{r})$ present as a rigid, density-independent external potential. In analogy to the static case,[5] one then has, instead of relation (15),

$$\int d^3r \, n_+(\mathbf{r})\nabla\phi(\mathbf{r},\omega) + \int d^3r \, n(\mathbf{r})\nabla V_{\text{xc}}(\mathbf{r})$$
$$= \omega^2 \int d^3r \, \mathbf{r} \, \delta n(\mathbf{r},\omega) . \tag{51}$$

Following the same derivation as above, we obtain, for the centroid of the screening density, the expression

$$d(\omega) = \frac{\epsilon(\omega) + 1}{\epsilon(\omega)} \left[\int_0^\infty dz \, z \, \delta n(z,\omega) \right.$$
$$\left. - \omega_p^{-2} \int_{-\infty}^\infty dz \, \delta n(z,\omega) V'_{\text{xc}}(z) \right] \tag{52}$$

instead of Eq. (31). The induced density is, in this case, determined from the same set of response equations (11)–(14), except that the exchange-correlation term $\delta V_{\text{xc}}(z,\omega)$ is omitted from the self-consistent potential $\phi_{\text{SCF}}(z,\omega)$.

IV. CALCULATIONAL PROCEDURE

The method we have used to solve Eqs. (11)–(14) is similar to the procedure employed previously at purely

imaginary frequencies.[9] However, since $\delta n(z,\omega)$ at real ω is complex, several additional points must be addressed. Using the decomposition of the total Coulomb potential given in (47), we introduce the function

$$\xi(z,\omega) = \int dz' \, \chi_0(z,z',\omega)\phi_b(z',\omega)$$
$$= -2\pi[1 - \sigma(\omega)] \int_{-\infty}^\infty dz' \, z' \chi_0(z,z',\omega) . \tag{53}$$

The second expression follows from the identity[9]

$$\int dz' \, \chi_0(z,z',\omega + i\delta) = 0 , \tag{54}$$

where δ is a positive infinitesimal. Since

$$\frac{\kappa}{2} \int dz' \, e^{-\kappa|z - z'|} [z' - d(\omega)] = z - d(\omega) , \tag{55}$$

the surface part ϕ_s of ϕ satisfies the relation

$$\phi_s(z,\omega) = \int_{-\infty}^\infty dz' \, e^{-\kappa|z - z'|}$$
$$\times \left[\frac{2\pi}{\kappa} \delta n(z',\omega) + \frac{\kappa}{2}\phi_s(z',\omega) \right] , \tag{56}$$

and $\phi_s(z,\omega)$ is taken to vanish in the interior of the metal. Far from the surface ϕ_s has the form

$$\phi_s(z,\omega) = -4\pi\sigma(\omega)[z - d(\omega)], \quad z \gg 0 . \tag{57}$$

In order to account explicitly for this asymptotic behavior, it is convenient to write

$$\delta n(z,\omega) = \delta n_0(z,\omega) + \delta n_1(z,\omega) , \tag{58}$$

$$\phi_s(z,\omega) = \delta\phi_0(z,\omega) + \delta\phi_1(z,\omega) , \tag{59}$$

where δn_0 represents a complex model density whose real part is a Gaussian with total weight $\sigma(\omega)$:

$$\text{Re}\,\delta n_0(z,\omega) = \sigma(\omega)\frac{\Gamma}{\sqrt{\pi}}e^{-(z - d_0)^2\Gamma^2} . \tag{60}$$

Since $\sigma(\omega)$ is real, the imaginary part of δn_0 is represented by a "dipolar" distribution of the form

$$\text{Im}\,\delta n_0(z,\omega) = \sigma(\omega)\frac{d_1}{z_1 - z_2}\frac{\Gamma}{\sqrt{\pi}}$$
$$\times (e^{-(z - z_1)^2\Gamma^2} - e^{-(z - z_2)^2\Gamma^2}) . \tag{61}$$

The complex Coulomb potential $\delta\phi_0$ corresponding to δn_0 is defined as

$$\delta\phi_0(z,\omega) = -4\pi \int_{-\infty}^z dz'(z - z')\delta n_0(z',\omega)$$
$$\to -4\pi\sigma(\omega)(z - d_0 - id_1), \quad z \gg 0 . \tag{62}$$

Having specified δn_0 and $\delta\phi_0$ in this manner, the response equations for the remaining functions δn_1 and $\delta\phi_1$ now read as follows:

$$\delta n_1(z,\omega) = \Delta(z,\omega)$$
$$+ \int dz' \, \chi_0(z,z',\omega)$$
$$\times [\delta\phi_1(z',\omega) + V'_{\text{xc}}(z')\delta n_1(z',\omega)] , \tag{63}$$

$$\delta\phi_1(z,\omega) = \int dz'\, e^{-\kappa|z-z'|}$$

$$\times \left[\frac{2\pi}{\kappa}\delta n_1(z',\omega) + \frac{\kappa}{2}\delta\phi_1(z',\omega) \right] , \quad (64)$$

where $\Delta(z,\omega)$ is defined as

$$\Delta(z,\omega) = \xi(z,\omega) - \delta n_0(z,\omega)$$

$$+ \int dz'\, \chi_0(z,z',\omega)$$

$$\times [\delta\phi_0(z',\omega) + V'_{xc}(z')\delta n_0(z',\omega)] . \quad (65)$$

Equations (63) and (64) provide the basis for the numerical results which will be discussed in the next section. By discretizing all functions on a mesh of points z_i, one obtains the matrix equation

$$\begin{bmatrix} 1 - \chi_0 V'_{xc}w & -\chi_0 w \\ -4\pi\kappa^{-2}Kw & 1-Kw \end{bmatrix} \begin{bmatrix} \delta n_1 \\ \delta\phi_1 \end{bmatrix} = \begin{bmatrix} \Delta \\ 0 \end{bmatrix} , \quad (66)$$

where

$$K(z,z') = \tfrac{1}{2}\kappa\exp(-\kappa|z-z'|) , \quad (67)$$

and w denotes integration weight factors.

Since δn_0 and $\delta\phi_0$ are, by definition, finite only in the surface region, the integral over z' in (65) can be done numerically. The z' integral which defines the function $\xi(z,\omega)$, Eq. (53), however, should be carried out before the internal momentum summation involved in the expression for χ_0:

$$\chi_0(z,z',\omega) = \frac{1}{\pi^2}\int_0^{k_F} dk\,(k_F^2-k^2)\psi_k(z)\psi_k(z')$$

$$\times [G(z,z',\varepsilon_k+\omega+i\delta)$$

$$+ G(z,z',\varepsilon_k-\omega-i\delta)] , \quad (68)$$

where $\psi_k(z)$ is a solution of the Schrödinger equation for the ground-state effective potential $V(z)$ and G is the corresponding Green function (see Ref. 9). Since the functions ψ_k and G are known analytically deep inside the metal, the z' integration in Eq. (53) can also be done analytically in this region.

The center position d_0 of the real part of δn_0 and the coefficient d_1, which characterizes $\mathrm{Im}\delta n_0$, will be used as input parameters. If the integrated weight and the first moment of δn_1 vanish, $\delta\phi_1$ does not have any long-range contributions and no truncation errors arise from Eq. (64). In this case

$$d(\omega) = d_0 + id_1 , \quad (69)$$

i.e., a self-consistent solution has been found. This solution must be independent of the range parameter κ, of the width Γ, and of the parameters z_1 and z_2 which enter in the definition of δn_0. In practice we solve (66) for two values of d_0 and of d_1. In these four cases $d(\omega)$ is calculated from the external part of $\delta n = \delta n_0 + \delta n_1$ by making use of the dynamical force sum rule, i.e., by applying Eq. (32). It is then straightforward to locate by interpolation that pair of values of d_0, d_1 which satisfies

Eq. (69). We have found this procedure to work very well in the entire frequency range up to ω_p. Further details concerning integration range, mesh size, momentum sums, etc. can be found in Ref. 9.

V. RESULTS AND DISCUSSION

Figure 1 shows the real and imaginary parts of the normalized induced density $f(z,\omega) = \delta n(z,\omega)/\sigma(\omega)$ for $r_s = 4$ at several frequencies below ω_p. Note that, with this normalization, the real part of $f(z,\omega)$ has unit integrated weight independently of ω. The total weight of the imaginary part of δn vanishes since there is no bulk damping included in the present theory. Both real and imaginary parts of $f(z,\omega)$ are seen to vary smoothly with frequency even though $\sigma(\omega)$ has a pole at the surface plasma frequency. $\mathrm{Re}f(z,\omega)$ consists of a main peak whose centroid is located outside the surface at low frequencies and which gradually shifts inwards as ω increases. This indicates that the screening of the applied field at higher frequencies takes place in regions of higher electronic density, i.e., in regions of larger "local" Fermi wave vectors. At the same time, $\mathrm{Re}f(z,\omega)$ becomes negative at large z, suggesting that the applied field is antiscreened in the tail region of the ground-state density profile at sufficiently high frequencies.

In the interior, $\mathrm{Re}f(z,\omega)$ exhibits various Friedel oscillations[3] in contrast to its behavior at purely imaginary frequencies where, as in the static limit, only one oscillation of wavelength π/k_F is obtained.[9] At small real ω the dominant period is given by

$$\lambda_1 = 2\pi/[k_F + (k_F^2 + 2m\omega/\hbar)^{1/2}] ,$$

which is gradually replaced by a longer-wavelength oscillation given by $\lambda_2 = 2\pi\hbar k_F/m\omega$. While close to the surface plasma frequency (see curve at $0.7\omega_p$) both periods are still discernible, the induced density at $0.8\omega_p$ appears to consist mainly of one period given almost exactly by λ_2. The amplitudes of the oscillations at this frequency are much larger than at other values of ω.

The behavior of the imaginary part of $f(z,\omega)$ is qualitatively similar to that of the real part except that the overall magnitude of the extrema varies much more strongly with frequency (notice the different scales used at different values of ω). As before, close to $\omega_s = \omega_p/\sqrt{2}$ the induced density is still quite complicated, consisting at least of the two oscillations λ_1 and λ_2 specified above. At $\omega = 0.8\omega_p$, however, $\mathrm{Im}f(z,\omega)$ takes on a very simple form with a large "dipole" near the jellium edge and strong Friedel oscillations in the interior corresponding to the wavelength λ_2. Similar variations of $f(z,\omega)$ with frequency are found for other bulk densities.

The real and imaginary parts of the centroid $d(\omega)$ of the induced density are plotted in Fig. 2 as functions of frequency for bulk densities corresponding to $r_s = 2$, 3, 4, and 5. [The numerical values of $\mathrm{Im}d(\omega)$ are given in Table I.] Both $\mathrm{Re}d(\omega)$ and $\mathrm{Im}d(\omega)$ clearly exhibit two spectral features below ω_p. The first is related to the threshold for emission and leads to structure in $d(\omega)$ at frequencies near the work function Φ (see vertical arrows). At very low frequencies, $\mathrm{Im}d(\omega)$ increases linear-
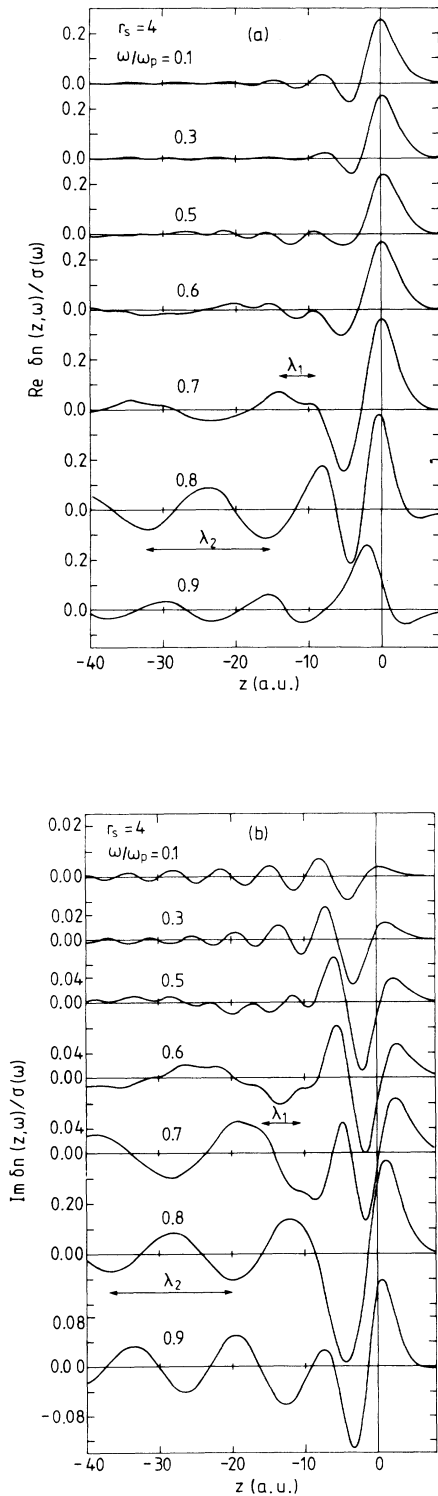
FIG. 1. (a) Real and (b) imaginary parts of normalized density Eq. (37), induced at a metal surface by a uniform electric field oriented normal to the surface. The positive background occupies the half-space $z \leq 0$. The principal short- and long-wavelength Friedel oscillations in the interior are indicated by λ_1 and λ_2, respectively. Notice the different scales in (b).
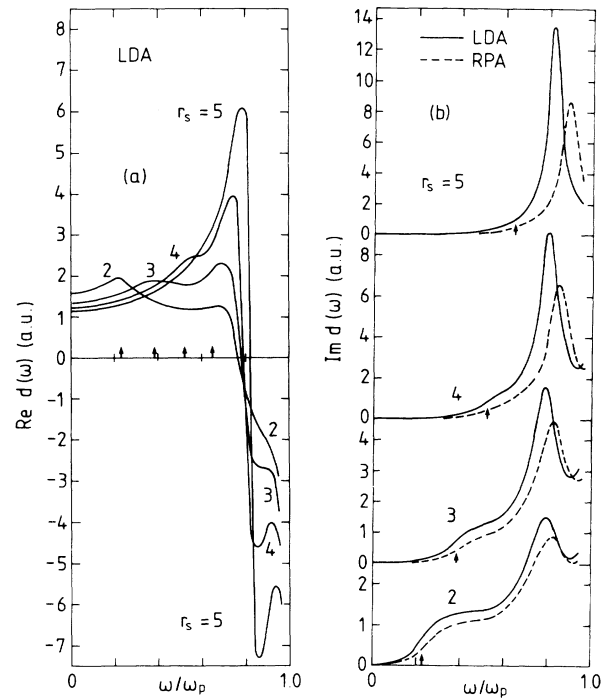
FIG. 2. (a) Real and (b) imaginary parts of centroid $d(\omega)$ of density induced at several simple-metal surfaces. The vacuum threshold is marked by the vertical arrows. Solid lines; TDLDA; dashed lines in (b), LDA-based RPA.

ly, since the phase space for electron-hole pair excitations grows proportionally with ω. In the vicinity of the threshold for emission into the vacuum, $\text{Im}d(\omega)$ increases steeply, suggesting that many additional excitation channels are opened up once states near the top of the surface barrier can be reached.

It should be noted that in spite of the complicated spatial distribution of the induced density, all of the information on $d(\omega)$ is, as a result of the dynamic force sum rule, contained in the external part of $\delta n(z,\omega)$. Combining Eqs. (37)–(39) we find

$$d(\omega) = (1 - \bar{\omega}^2)^{-1} \int_0^\infty dz \, z \, \delta n(z,\omega)/\sigma(\omega) . \qquad (70)$$

For example, the rise of $\text{Im}d(\omega)$ near threshold for $r_s = 4$

TABLE I. $\text{Im}d(\omega)$ as a function of ω/ω_p for several bulk densities (a.u.).

ω/ω_p	$r_s = 2$	$r_s = 3$	$r_s = 4$	$r_s = 5$
0.1	0.11	0.04	0.02	0.01
0.2	0.45	0.11	0.05	0.03
0.3	1.05	0.30	0.12	0.06
0.4	1.30	0.87	0.28	0.11
0.5	1.35	1.23	0.71	0.30
0.6	1.62	1.63	1.38	0.71
0.7	2.41	2.93	2.66	1.82
0.8	3.62	5.55	9.08	10.80
0.9	2.66	2.87	2.94	3.28

($\Phi = 0.52\omega_p$) can be identified both with an increased magnitude of $\text{Im} f(z,\omega)$ in the exterior and with an outward shift. Thus more unoccupied states near the top of the surface barrier are involved in the formation of electron-hole pairs in this frequency range.

A second, more dramatic increase of $\text{Im} d(\omega)$ occurs at about $0.8\omega_p$ for all r_s that we have investigated. This peak is accompanied by typical resonance behavior in $\text{Re} d(\omega)$. The peak in $\text{Im} d(\omega)$ is relatively broad for low r_s but becomes extremely sharp for $r_s = 4$ and 5. In these two systems, the rise near threshold shows itself merely as a shoulder of the main peak since Φ approaches $0.8\omega_p$. As can be seen from Fig. 1(a), the external part of $f(z,\omega)$ is a smooth function of frequency. Its moment $f(\omega)$ is negative and finite as ω approaches ω_p. Thus, according to Eq. (70), $\text{Re} d(\omega) \rightarrow -\infty$ as $\omega \rightarrow \omega_p$. This implies that, since $\text{Re} d(\omega) > 0$ for $\omega < \omega_s$, $\text{Re} d(\omega)$ must pass through zero somewhere between ω_s and ω_p. Now, if the centroid of the induced density lies close to the jellium edge, i.e., close to the steepest part of the barrier potential, the probability for electron-hole pair excitation will be large as a result of an enhanced local field. Thus $\text{Im} d(\omega)$ should become large where $\text{Re} d(\omega)$ goes through zero. This is indeed the case, as shown in Fig. 2. Moreover, according to the Kramers-Kronig relations, a peak in $\text{Im} d(\omega)$ implies resonance-type structure in $\text{Re} d(\omega)$, which is also borne out by the results presented in Fig. 2(a).

The normalized Coulomb potential $\phi(z,\omega)/\sigma(\omega)$ corresponding to the induced density $\delta n(z,\omega)/\sigma(\omega)$ for $r_s = 4$ is shown in Fig. 3 for frequencies near the resonance. As ω increases from $0.7\omega_p$ to $0.9\omega_p$, the maximum of the real part is seen to move through the jellium edge, so that, at resonance, the spatially most inhomogeneous part of $\phi(z,\omega)$ has maximum overlap with the spatially most inhomogeneous region of the ground-state potential. Whereas the overall magnitude of $\text{Re}\phi(z,\omega)/\sigma(\omega)$ varies relatively little in this frequency range, $\text{Im}\phi(z,\omega)/\sigma(\omega)$ is seen to show the same kind of resonance behavior as the imaginary part of the induced density. Note that condition (50), which follows from the dynamical force sum rule, is quite well satisfied by the curves shown in Fig. 3.

The observation that the resonances in $d(\omega)$ occur above ω_s for all bulk densities considered here is presumably related to the fact that, for $\omega < \omega_s$, the induced potential in the interior and ϕ_{ext} oscillate out of phase [see the definition (1)], i.e., they partially cancel. Above ω_s the integrated surface charge becomes negative, so that $\delta\phi$ and ϕ_{ext} oscillate in phase and the total field is able to penetrate the interior much more efficiently. Thus the screening charge will no longer be confined to the surface region and begins to spread into the metal. A resonance condition then arises when the centroid of the screening cloud coincides with the steepest portion of the ground-state potential.

Note that the integrated weight of the normalized induced density $f(z,\omega)$ is unity independently of frequency. Thus the resonance near $0.8\omega_p$ has monopole character just as the spatial distribution of the surface plasmon (compare the curves at $0.7\omega_p$ and $0.8\omega_p$ in Fig.

1). In contrast to these induced densities which characterize the driven response of the electrons, Inglesfield and Wikborg[17] investigated the self-sustained modes of a semi-infinite metal. For a particular double-step surface potential model, they obtain damped modes of vanishing total weight at a frequency close to $0.8\omega_p$.
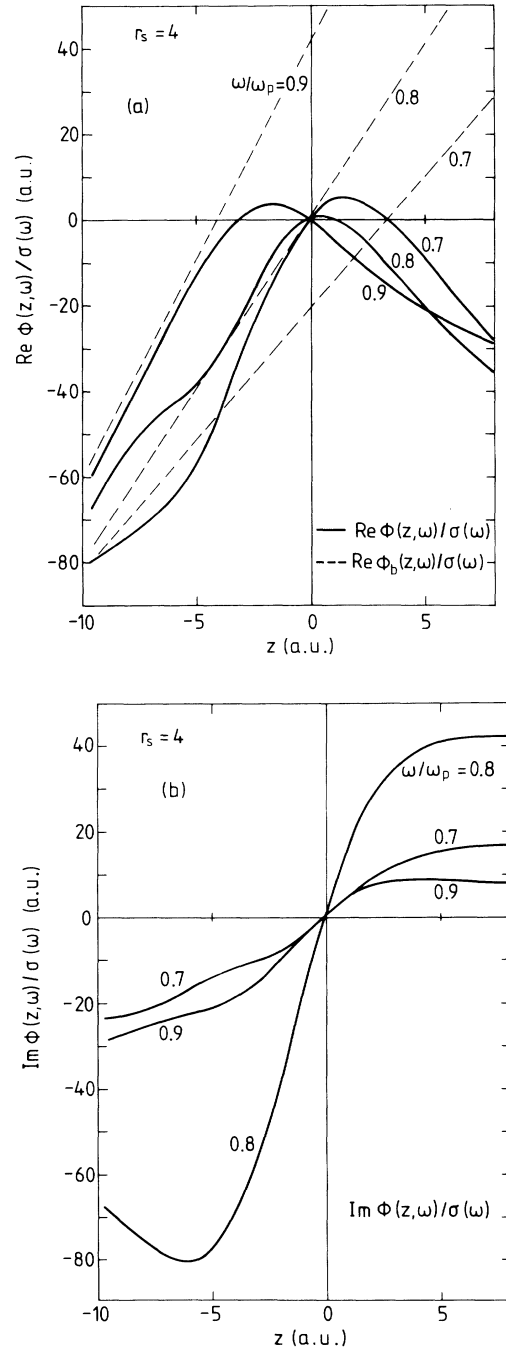
FIG. 3. (a) Real and (b) imaginary parts of the Coulomb potential, Eq. (47), for several frequencies near resonance. The dashed lines in (a) denote the bulk contribution defined in Eq. (48). All curves are divided by $\sigma(\omega)$ to ensure the same normalization as in Fig. 1.

Figure 2(b) demonstrates that the resonance near $0.8\omega_p$ is sharpest for low-density metals whose density profile at the surface is more diffuse. It is therefore not surprising that finite- or infinite-barrier models show no resonance, since their density profile for typical bulk densities tends to be too steep.[18,19] In the case of the infinite-barrier model, only systems with $r_s > 15$ have sufficiently soft electron distributions that resonances in $d(\omega)$ begin to occur. However, we hesitate to associate the resonances near $0.8\omega_p$ with a "local" plasma oscillation in the tail of the ground-state electron profile. According to the induced densities shown in Fig. 1, the spatial distribution of $\delta n(z,\omega)$ at $0.8\omega_p$ is not more concentrated in the surface region than at other frequencies. Also, the Friedel oscillations at this frequency are as much amplified as the main peak near the jellium edge and as the imaginary part of the centroid $d(\omega)$. The only clear feature that distinguishes the induced density profile at $0.8\omega_p$ from those at other frequencies is the fact that the oscillatory part is dominated by the term with wave vector $m\omega/\hbar k_F$ and that $\text{Im}\delta n(z,\omega)$ acquires a pronounced dipolar shape in the surface region.

As can be seen from Fig. 2(b), the maximum of $\text{Im}d(\omega)$ shifts to slightly higher frequencies as r_s increases (from about $0.78\omega_p$ for $r_s = 2$ to $0.82\omega_p$ for $r_s = 5$). Interpreting these frequencies as local plasma frequencies and converting them into local plasma densities, one finds that these densities happen to be equal to the ground-state density approximately where this has its largest gradient (from $z \approx -0.3$ a.u. for $r_s = 2$ to $z \approx -1.1$ a.u. for $r_s = 5$). This upward shift of the resonance frequency is consistent with the fact that $d(0)$ is a decreasing function of r_s. From the Kramers-Kronig relations we have

$$d(0) = \frac{2}{\pi} \int_0^\infty d\omega \, \text{Im}d(\omega)/\omega . \tag{71}$$

Thus if $\text{Im}d(\omega)$ were to consist of a narrow peak of unit strength located at a frequency ω_0, $d(0)$ and ω_0 should be approximately inversely related. Also, as a result of the surface f-sum rule,[20,21] one has the relation

$$\lambda\omega_p^2 = \frac{2}{\pi} \int_0^\infty d\omega \, \text{Im}d(\omega) , \tag{72}$$

where λ is a ground-state quantity defined as

$$\lambda = \int_0^\infty dz \, n_0(z)/\bar{n} . \tag{73}$$

The upward shift of the main peak of $\text{Im}d(\omega)$ as r_s increases is consistent with the fact that λ is an increasing function of r_s.[5] [Integrating $\text{Im}d(\omega)/\omega$, and $\omega\,\text{Im}d(\omega)$ up to ω_p and comparing the result with the values of $d(0)$ and λ, we find that, nearly independently of r_s, about 120% of the total weight of $\text{Im}d(\omega)/\omega$ and 160% of the total weight of $\omega\,\text{Im}d(\omega)$ lie below ω_p, respectively. Note that $\text{Im}d(\omega)$ becomes negative above ω_p.]

The dashed lines in Fig. 2(b) show $\text{Im}d(\omega)$ for an LDA ground-state description and an RPA-type response treatment. There is an almost uniform shift of spectral weight to higher frequencies and a reduction of amplitude. Since the main peak in $\text{Im}d(\omega)$ lies at higher frequencies, the resonance-type structure in $\text{Re}d(\omega)$ near

$0.8\omega_p$ lies closer to the singularity at ω_p and is therefore less well resolved than in the time-dependent LDA (TDLDA). As we have shown previously,[5] the neglect of exchange-correlation terms from the self-consistent potential makes this slightly less attractive and therefore leads to a shift of the static image plane position $d(0)$ towards the surface. According to the Kramers-Kronig relation (71) this displacement is consistent with the upward shift of the main peak of $\text{Im}d(\omega)$. A shift to higher frequencies due to the neglect of δV_{xc} was also obtained in atomic absorption spectra.[6] On the other hand, the LDA-based RPA values of λ are smaller than the consistently calculated values.[5] This implies that the overall weight of $\text{Im}d(\omega)$, in particular above ω_p, must be underestimated appreciably by the RPA-type response treatment.

For those values of r_s (2, 3, and 4) and at those frequencies ($0.6 < \omega/\omega_p < 1.0$) where a comparison is possible, our results for $d(\omega)$ agree very well with those of Feibelman (Figs. 9 and 10 of Ref. 1). In the case of Al ($r_s = 2$), incorporation of exchange-correlation contributions into the induced potential is seen to shift the main peak in $\text{Im}d(\omega)$ by about 0.5 eV to lower frequencies. Given the experimental uncertainties, it does not seem possible at present to conclude that the TDLDA agrees better with the measured photoyield spectra than the LDA-based RPA. It would be of great interest to perform photoyield measurements on the low-density simple metals to verify the local-field enhancement near $0.8\omega_p$ and to check whether the experimental data can discriminate between the theoretical peak positions obtained within the LDA and RPA. For Na and K ($r_s \approx 4$ and 5), the time-dependent LDA predicts maxima in the photoyield at about 4.7 and 3.5 eV, while the LDA-based RPA gives peaks at 5.0 and 3.8 eV, respectively. Also, it would be interesting to measure the dispersion of the energy and width of the surface plasmon, since at small wave vectors these quantities are directly determined by $d(\omega_s)$:[1]

$$\omega_s(q) = \omega_s[1 - \tfrac{1}{2}qd(\omega_s) + O(q^2)] . \tag{74}$$

A comparison of the numerical values of $d(\omega_s)$ in the LDA and RPA is given in Table II.

We conclude the presentation of our results with a discussion of the low-frequency behavior of $d(\omega)$, which is relevant for low-energy inelastic scattering of electrons from surfaces and the damping of adsorbate vibrations. At small frequencies $\text{Im}d(\omega)$ is proportional to ω:[14]

$$\text{Im}d(\omega) = \xi\omega/\omega_p, \quad \omega \ll \omega_p . \tag{75}$$

TABLE II. $\text{Re}d(\omega_s)$ and $\text{Im}d(\omega_s)$ for several bulk densities in TDLDA and LDA-based RPA (a.u.).

	$r_s = 2$	$r_s = 3$	$r_s = 4$	$r_s = 5$
$[\text{Re}d(\omega_s)]_{\text{LDA}}$	1.2	2.3	3.6	4.2
$[\text{Im}d(\omega_s)]_{\text{LDA}}$	2.5	3.2	3.0	2.0
$[\text{Re}d(\omega_s)]_{\text{RPA}}$	0.8	1.4	1.7	1.4
$[\text{Im}d(\omega_s)]_{\text{RPA}}$	2.1	2.2	1.6	1.0

Since Re$d(\omega)$ is an even function of ω, the coefficient ξ may also be determined from the linear slope of the induced charge centroid at small imaginary frequencies:[20]

$$d(iu) = d(0) - \xi u / \omega_p, \quad u \ll \omega_p . \tag{76}$$

In Ref. 9 we determined these slopes by numerically evaluating the first moment of $\delta n(z, iu)$ both inside and outside the jellium edge. Using the dynamical force sum rule, $d(iu)$ can be calculated more reliably, since the evaluation of the moment of the oscillatory internal part is avoided. The low-frequency behavior of $d(iu)$ and of the real and imaginary parts of $d(\omega)$ is illustrated in Fig. 4. The dashed lines indicate the linear slope of $d(iu)$ and of Im$d(\omega)$ in the static limit. Although the new results for $d(iu)$ agree at all frequencies with the old ones to within about 1%, the slopes at small u are now much smaller because of the presence of a quadratic term which had been ignored before. Since the procedure described in Sec. III works well also at very small real frequencies, we calculate ξ both from Eqs. (75) and (76), and find the values given in Table III.

Remarkably, these new values agree very well with the quasistatic gold-rule results (see Fig. 7 of Ref. 9). Thus we have confirmed the validity of the approach of Persson and Zaremba,[14] who calculate the transition rate for electron-hole pair excitations at low frequencies by approximating the total complex potential in the golden rule, Eq. (10), by a superposition of the finite-frequency bulk potential and the static limit of the surface potential. It is crucial, however, to take not only the Hartree term of the surface potential but to include also exchange-correlation terms. Omission of these contributions leads, as was shown in Ref. 9, to an incorrect variation of ξ with bulk density. (Accidentally, the curves cross near $r_s = 2.55$, quite close to the r_s value of Cu, $r_s = 2.67$.)

In the LDA-based RPA, the low-frequency slopes of Im$d(\omega)$ are much smaller than in the consistent time-dependent LDA (see Table III). These values also agree with the corresponding quasistatic golden-rule coefficients. (See Fig. 7 of Ref. 9.)

The good agreement between the dynamical results for ξ and those obtained from the quasistatic golden-rule approach is rather impressive in view of the very large can-

TABLE III. Low-frequency coefficient ξ of Im$d(\omega)$ for several bulk densities in TDLDA and LDA-based RPA. Also given are the bulk, surface, and interference contributions to ξ and its total value in the quasistatic approximation for the TDLDA (a.u.).

	$r_s = 2$	$r_s = 3$	$r_s = 4$	$r_s = 5$
ξ_{LDA}	0.85	0.32	0.17	0.10
ξ_{RPA}	0.55	0.14	0.04	0.01
ξ_b	1.18	1.44	1.66	1.81
ξ_s	2.37	2.06	2.08	2.20
$-\xi_i$	2.73	3.18	3.57	3.91
ξ_{tot}	0.82	0.32	0.17	0.10
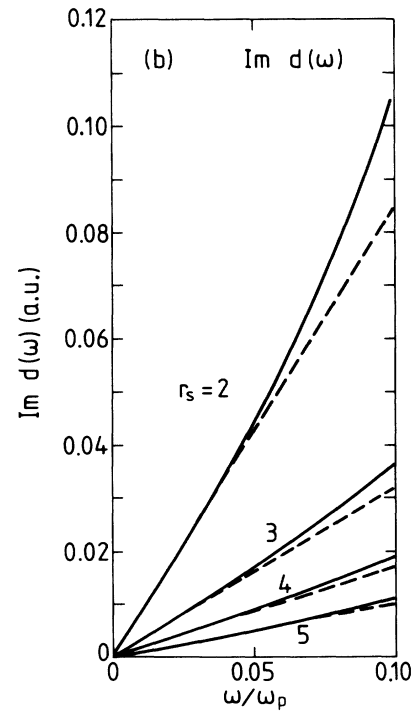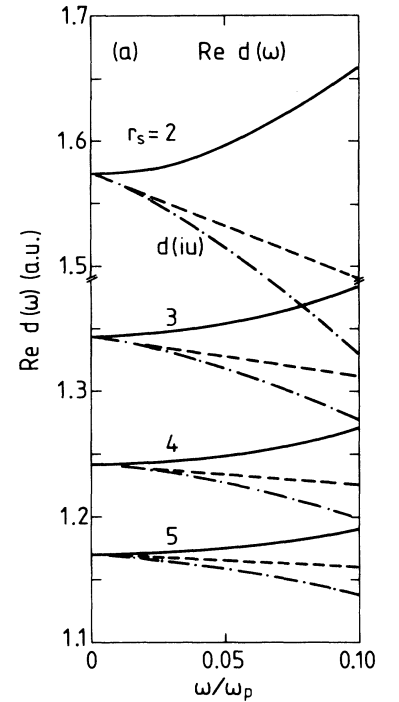
FIG. 4. (a) Real and (b) imaginary parts of $d(\omega)$ at low frequencies. The dot-dashed curves in (a) represent the behavior of the centroid at small imaginary frequencies $\omega = iu$. The dashed lines in (a) and (b) indicate the linear variation of $d(iu)$ and Im$d(\omega)$ in the static limit.

cellations between bulk, surface, and interference terms that occur in this latter method. Typically, the individual bulk and surface contributions to the transition rate are much larger than the true rate (see Table III). It is therefore very important to account for the coherence of bulk- and surface-related excitations and not to treat them as independent processes.

VI. CONCLUSION

In this paper we have calculated the dynamic image plane for several metal surfaces. The nonlocal response of the electron distribution at finite real frequencies is obtained using the time-dependent density-functional approach. Electron-electron interactions in the presence of the external perturbation are therefore treated on the same level of approximation as in the ground state. Generalizing the dynamical force sum rule to semi-infinite systems, we have shown that the dynamic image plane is given identically by the first moment of the induced density in the region outside the positive ionic background.

The method which we use to solve for the induced density is an extension of the one previously employed at purely imaginary frequencies. By carefully separating bulk and surface contributions to the self-consistent complex potential we are able to solve the linear-response equations directly at all frequencies below the bulk plasma frequency. We have shown that the transition rate for electron-hole pair creation, which is determined by the imaginary part of the induced charge centroid, rises steeply near the threshold for emission and exhibits a peak at about $0.8\omega_p$. The real part of $d(\omega)$ shows, in this region, the typical resonance behavior that is to be expected on the basis of the Kramers-Kronig relations. The spatial distribution of the induced density at this frequency is qualitatively similar to that at other values of ω. In particular, it has monopole character and is globally enhanced, not only in the surface region. Physically, this spectral features seems to correspond to an enhanced local field when the centroid of the induced density crosses the steepest part of the ground-state potential.

We have also carried out RPA-type response calculations and found excellent agreement with earlier results by Feibelman. We have shown that the neglect of exchange-correlation terms in the effective potential leads to an upward shift of spectral weight by only a few tenths of an eV. Thus the TDLDA supports the interpretation of the photoyield spectra for Al in terms of an enhanced local field. On the other hand, the values of $d(\omega)$ at specific frequencies can differ appreciably between RPA and consistent LDA. For example, in the case of Na the real and imaginary parts of $d(\omega_s)$ are 50% smaller in the RPA than the LDA values. This could be checked experimentally by measuring the dispersion of the energy and width of the surface plasmon in the limit of small parallel wave vectors.

Finally, we have examined the behavior of $\mathrm{Im}d(\omega)$ at small frequencies and find a linear coefficient ξ consistent with that of $d(iu)$ at small imaginary frequencies. The present values of ξ are more accurate than those calculated previously, since the dynamical force sum rule permits a more reliable determination of the induced charge centroid. In fact, we now obtain a very good agreement with the linear coefficients predicted from the quasistatic golden-rule approach. It is important, however, to calculate the transition-matrix elements using the full surface potential (i.e., including exchange-correlation terms) together with the frequency-dependent bulk potential.

Note added in proof. As shown recently by Kempa and Schaich, the main long-wavelength Friedel oscillation at finite frequencies is in fact caused by transitions to the vacuum threshold. Thus its wavelength is given by (a.u.) $\lambda = 2\pi/[\sqrt{2V} - \sqrt{2(V-\omega)}]$ where V is the total barrier height. Accidentally, this wavelength is very similar to $\lambda_2 = 2\pi k_F/\omega$ (see text) for the frequencies and bulk densities discussed in the present work.

[1]P. J. Feibelman, Prog. Surf. Sci. **12**, 287 (1982).

[2]A. Liebsch, Phys. Scr. **35**, 354 (1987).

[3]P. J. Feibelman, Phys. Rev. B **12**, 1319 (1975).

[4]H. Levinson, E. W. Plummer, and P. J. Feibelman, Phys. Rev. Lett. **43**, 952 (1979).

[5]A. Liebsch, Phys. Rev. B **32**, 6255 (1985).

[6]A. Zangwill and P. Soven, Phys. Rev. A **21**, 1561 (1980).

[7]M. J. Stott and E. Zaremba, Phys. Rev. A **21**, 12 (1980); G. D. Mahan, *ibid.* **22**, 1780 (1980).

[8]K. Kempa and W. L. Schaich (unpublished).

[9]A. Liebsch, J. Phys. C **19**, 5025 (1986).

[10]A. Liebsch, Phys. Rev. B **33**, 7249 (1986).

[11]R. S. Sorbello, Solid State Commun. **56**, 821 (1985).

[12]R. S. Sorbello, Solid State Commun. **48**, 989 (1983).

[13]A. Liebsch, Europhys. Lett. **1**, 361 (1986).

[14]B. N. J. Persson and E. Zaremba, Phys. Rev. B **31**, 1863 (1985).

[15]P. J. Feibelman, Phys. Rev. B **22**, 3654 (1980); **14**, 762 (1976); **9**, 5077 (1974).

[16]M. Manninen, R. Nieminen, P. Hautojärvi, and J. Arponen, Phys. Rev. B **12**, 4012 (1975).

[17]J. E. Inglesfield and E. Wikborg, J. Phys. F **5**, 1706 (1975).

[18]R. R. Gerhardts and K. Kempa, Phys. Rev. B **30**, 5704 (1984); K. Kempa and R. R. Gerhardts, Solid State Commun. **53**, 579 (1985).

[19]W. L. Schaich and K. Kempa, Phys. Scr. **35**, 204 (1987).

[20]B. N. J. Persson and E. Zaremba, Phys. Rev. B **30**, 5669 (1984).

[21]B. N. J. Persson and P. Apell, Phys. Rev. B **27**, 6058 (1983).